Electronic Supplementary Material (ESI) for Journal of Materials Chemistry A.

Supporting Information for

Cold plasma-activated AgCo surface in situ alloying for enhancing CO_2 electroreduction to ethanol

Qiang Zhang,‡[ab] Shuihui Tao,‡[cd] Jun Du,*[ab] Anbang He,[ab] Yong Yang[ab] and Changyuan Tao*[ab]

[a]*State Key Laboratory of Coal Mine Disaster Dynamics and Control, Chongqing University, Chongqing 400044, China.*
[b]*College of Chemistry and Chemical Engineering, Chongqing University, Chongqing 401331, China.*
[c]*Department of Chemistry, Xi'an Jiaotong-Liverpool University, Suzhou, Jiangsu, 215123, China.*
[d]*Department of Chemistry, University of Liverpool, Liverpool, L697ZD, UK.*

‡These authors contributed equally.
*Corresponding authors: College of Chemistry and Chemical Engineering, Chongqing University, Chongqing 401331, China.
E-mail addresses: dujune@cqu.edu.cn (Jun Du), taocy@cqu.edu.cn (Changyuan Tao).

Mailing address for correspondence:

Dr. Du, Jun (Prof.)

College of Chemistry and Chemical Engineering, Chongqing University

No.55 Daxuecheng South Rd., Shapingba

Chongqing 401331, China

Tel: +86-23-62678923

Fax: +86-23-62678923

E-mail: dujune@cqu.edu.cn

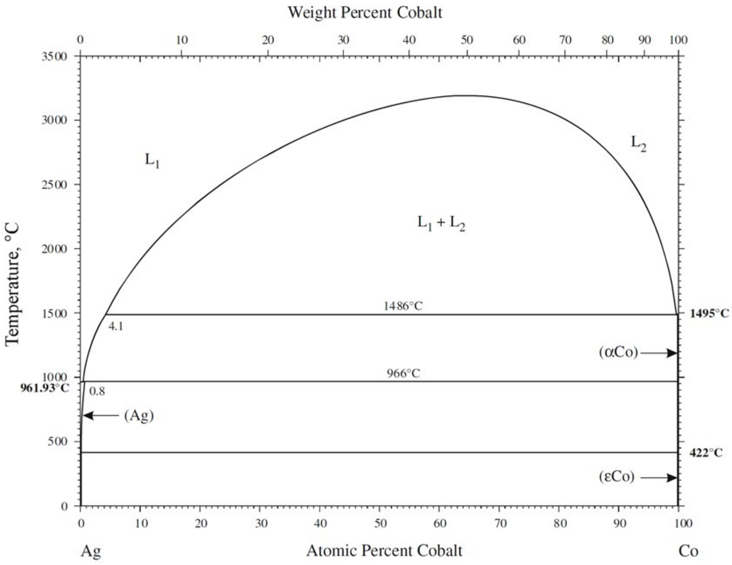

Fig. S1 Ag-Co phase diagram.[1]

When the content of cobalt atoms is 0.8%, the Ag-Co partial miscible alloying requires a very high temperature (961.93^{o}C).[1] The high temperature leads to agglomerate the metal catalyst, which is not conducive to the catalytic reaction. In order to solve this problem, we used a cold plasma (200 W 10 min) technology under room temperature to obtain AgCo surface alloy.

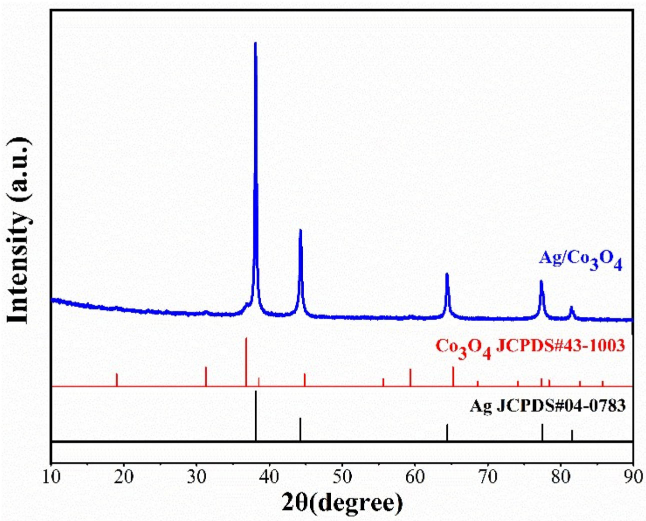

Fig. S2 XRD pattern of as-synthesized Ag/Co_3O_4 nanocubes.

The diffraction peaks of the Ag/Co_3O_4 nanocubes at 38.1°, 44.2°, 64.4°, 77.4° and 81.5° can be readily assigned to the (111), (200), (220), (311) and (222) crystal planes of Ag (JCPDS#04-0783, space group: *Fm-3m(225)*). The peak at 31.2°, 36.8° and 59.3° is also corresponding to the crystal planes of (220), (311) and (511) of Co_3O_4 (JCPDS#15-0806, space group: *Fm-3m(225)*).

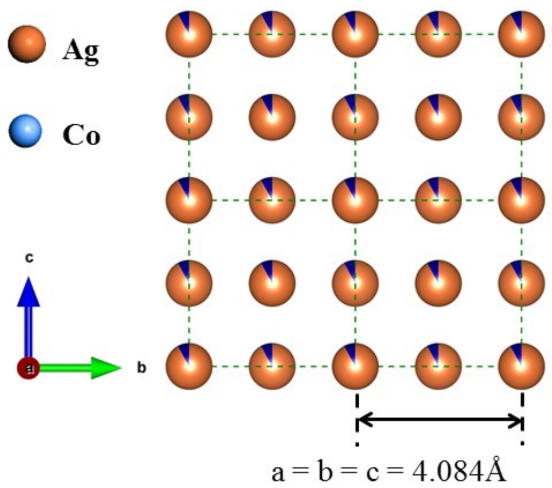

Fig. S3 General view of the face-centered-cubic crystal structure with parameters of a = b = c = 10.08 Å. Zeolitic water is omitted for clarity.

According to Rietveld calculations, the lattice parameter of AgCo SA (a=b=c= 4.084 Å) is slightly smaller than pure Ag (a=b=c= 4.086 Å), which can indicate that Co atom has been doped into the Ag lattice. The refined atomic coordinates and thermal parameters of AgCo SA are listed in Table S1. The occupancy of Ag is 0.92, and the occupancy of Co is only 0.08.

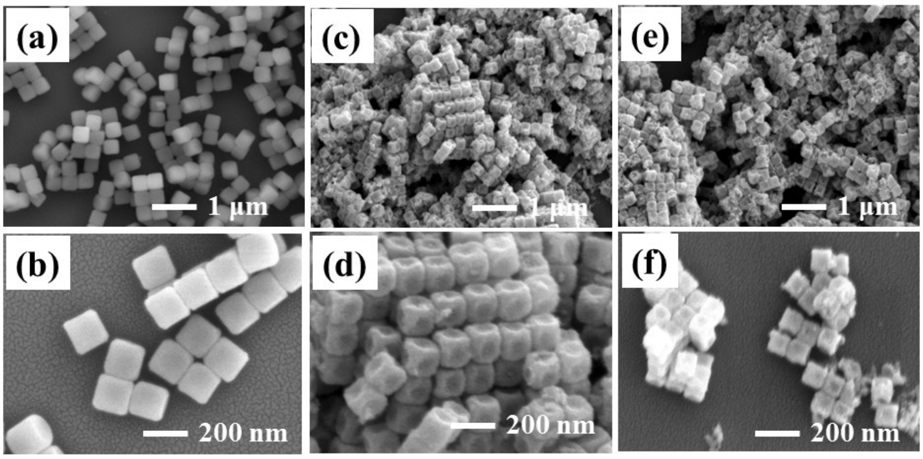

Fig. S4 FESEM images of the precursor $Ag_3Co(CN)_6$ (a-b), Ag/Co_3O_4 (c-d) and AgCo SA (e-f) at different magnification.

The FESEM images revealed that $Ag_3Co(CN)_6$ boxes were uniform in size with diameters ≈100-200 nm with smooth surface. After pyrolysis, Ag/Co_3O_4 submicroboxes were formed, which maintained the precursor's morphology with cube faces becoming concave, as a result of decomposition and volatilization of organic compounds. Moreover, after cold H_2-plasma treatment, resulting AgCo SA retained the submicroboxes shape with concave and the surfaces became very rough as shown in Fig. S4e-f.

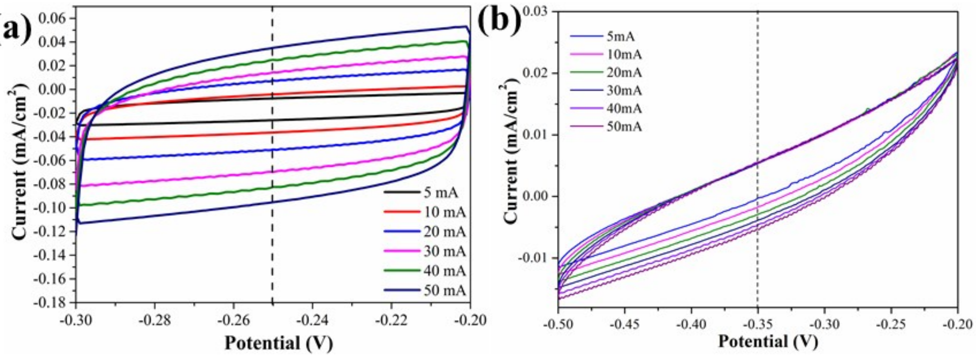

Fig. S5 CV curve of (a) AgCo SA and (b) pure Co electrode in 0.1 M $KHCO_3$ saturated with CO_2 over under different scan rate.

The high activity of AgCo SA is partly ascribed to the high electrochemical active area (ECSA), which represents the amount of active sites to a certain degree, normally, the ECSA can be approximated to the electrochemical double layer capacitance (EDLC). Not surprisingly, AgCo SA exhibits a higher EDLC than pure Co, indicating larger ECSA, followed by a great number of active sites on AgCo SA, which is an important contributor to the enhanced activity.

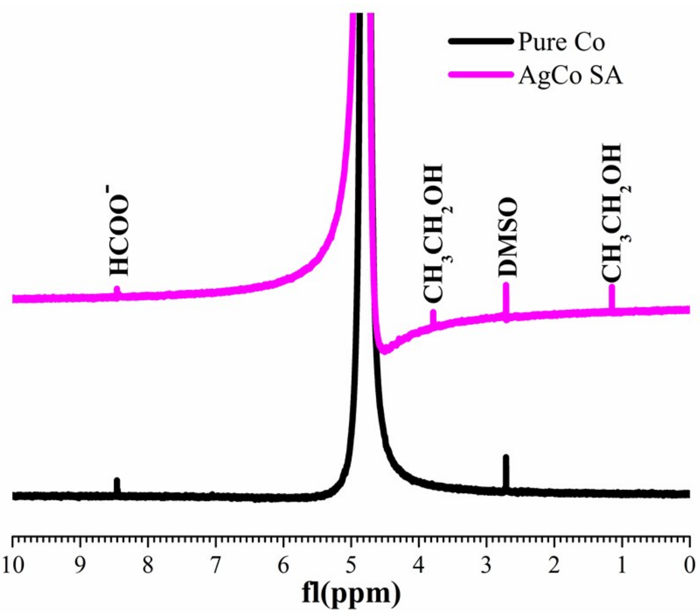

Fig. S6 ^{1}H-NMR of the aqueous products after the CO_2RR for 5 h at -0.8 V vs. RHE over AgCo SA and pure Co electrodes. The ^{1}H spectrum was tested with water suppression by a pre-saturation method. Typically, 0.1 mL of $KHCO_3$ solution after electrolysis was mixed with 0.1 mL of D_2O, which contained 0.05 μL of DMSO as an internal standard. The concentrations of formic acid and ethanol, were measured using an internal standard, DMSO (star, 2.5 ppm), to be 0.7 and 2.1 ppm, which were converted to the FEs of each product of 8.4% and 22.2%, respectively, in case of AgCo SA. The concentrations of formic acid were measured using an internal standard, DMSO (star, 2.5 ppm) to be 1.40 ppm, which were converted to the FEs of each product of 0.03%, respectively, in case of pure Co. Both data was analyzed by considering the total volume of the electrolyte (30 mL) and the total current, 7.4 mA•cm^{-2} (AgCo SA) and 4.9 mA•cm^{-2} (pure Co).

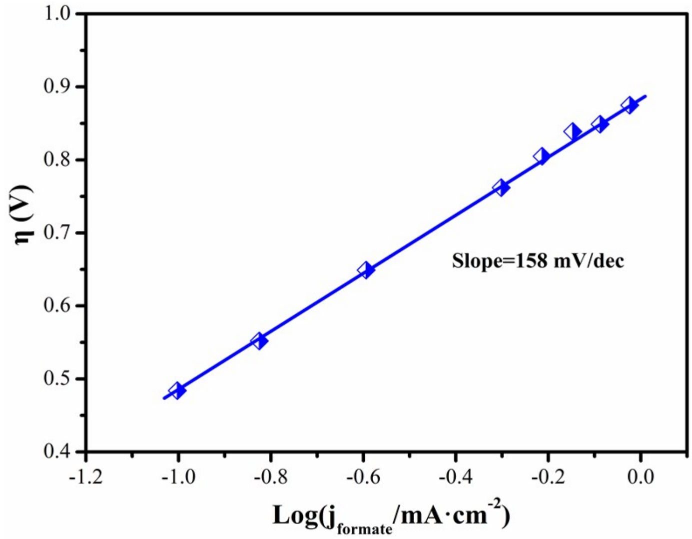

Fig. S7 Tafel plot for formate on pure Co electrodes in 0.1 M $KHCO_3$ solution.

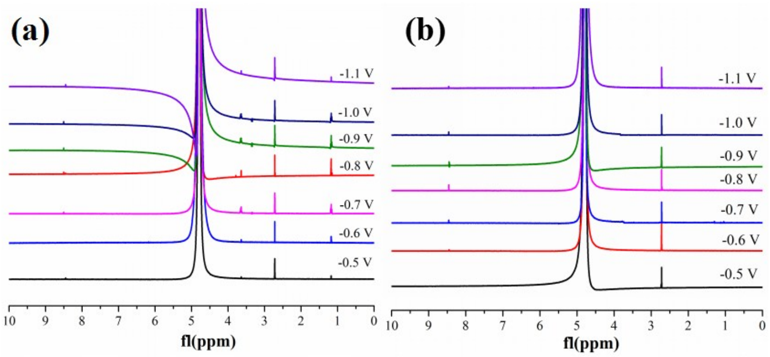

Fig. S8 ^{1}H-NMR of the aqueous products after the CO_2RR for 5 h at different potentials over AgCo SA (a) and pure Co (b).

Table S1 Structural parameters for AgCo SA in cubic system

Atom	x	y	z	g	Ueq(Å^2)
Ag1	0	0	0	0.92(3)	0.00009
Co1	0	0	0	0.08(3)	0.00158

Table S2 Electrochemical CO_2RR properties of AgCo SA compared with other electrocatalysts for ethanol production.

Catalysts		Electrolyte	Work potential	Current density (mA/cm^2)	Ethanol faradaic efficiency	Stability	Ref.
Bimetallic Alloy catalysts	CuAg alloy	1 M KOH	-0.7 V vs. RHE	300	25%	N.R.	2
	Cu_xZn alloy	0.1 M $KHCO_3$	-1.05 V vs. RHE	8.2	~29.1%	5 h	3
	$Au_{36}Cu_{64}$	0.5 M $KHCO_3$	-0.9 V vs. SCE	N.R.	~12%	N.R.	4
	AgCo SA	**0.1 M $KHCO_3$**	**-0.8 V vs. RHE**	**7.4**	**72.3%**	**~48 h**	**This work**
Other catalysts	Ag-G-NCF	0.1 M $KHCO_3$	-0.6 V vs. RHE	0.31	82.1%	10 h	5
	N-doped mesoporous carbon	0.1 M $KHCO_3$	-0.56 V vs. RHE	~0.25	77%	24 h	6
	Ag/Cu	1 M $KHCO_3$	-0.67 V vs. RHE	250	~41%	N.R.	7
	Plasma-activated Cu nanocube	0.1 M $KHCO_3$	-1.0 V vs. RHE	~34	~22%	N.R.	8
	Cu nanoparticles	0.1 M $KHCO_3$	-0.85 V vs. RHE	10	~17%	10 h	9
	Cu_2O	0.1 M $KHCO_3$	-0.99 V vs. RHE	35	~16%	60 h	10
	N-doped grapheme quantum dots	1 M KOH	-0.78 V vs. RHE	~23	~16%	N.R.	11
	Cu(B)-2	0.1 M $KHCO_3$	-1.1 V vs. RHE	~70	~27%	~36 h	12
	Cu_2S-Cu-V	1 M KOH	-0.92 V vs. RHE	120	~24.7%	~16 h	13
	Ag-Co_3O_4-CeO_2/LGC	0.1 M $KHCO_3$	-0.85 V *vs* RHE	12.8	54.2%	60 h	14
	Cu/TiO_2/NG	0.2 M KI	-0.75 V *vs* RHE	0.65	43.6%	20 h	15
	CuO/TiO_2	0.5 M $KHCO_3$	-0.85 V *vs* RHE	8.03	27.4%	25 h	16

N.R. : not reported

References

[1] H. Okamoto, J. Phase Equilib. Diff., 2015, 36, 10-21.

[2] T. T. H. Hoang, S. Verma, S. Ma, T. T. Fister, A. I. Frenkel, P. J. A. Kenis and A. A. Gewirth, J. Am. Chem. Soc., 2018, 140, 5791-5797.

[3] D. Ren, B. S. H. Ang and B. S. Yeo, ACS Catal., 2016, 6, 8239-8247.

[4] F. L. Jia, X. X. Yu, L. Z. Zhang, J. Power Sources, 2014, 252, 85-89.

[5] K. L. Lv, Y. C. Fan, Y. Zhu, Y. Yuan, J. R. Wang, Y. Zhu and Q. F. Zhang, J. Mater. Chem. A, 2018, 6, 5025-5031.

[6] Y. F. Song, W. Chen, C. C. Zhao, S. G. Li, W. Wei and Y. H. Sun, Angew. Chem. Int. Ed., 2017, 56, 10840-10844.

[7] Y. C. Li, Z. Y. Wang, T. G. Yuan, D. H. Nam, M. C. Luo, J. Wicks, B. Chen, J. Li, F. W. Li, F. P. García de Arquer, Y. Wang, C. T. Dinh, O. Voznyy, D. Sinton and E. H. Sargent, J. Am. Chem. Soc., 2019, 141, 8584-8591.

[8] D. F. Gao, I. Zegkinoglou, N. J. Divins, F. Scholten, I. Sinev, P. Grosse and B. R. Cuenya, ACS Nano, 2017, 11, 4825-4831.

[9] D. Kim, C. S. Kley, Y. F. Li and P. D. Yang, P. Natl. Acad, Sci. U. S. A., 2017, 114, 10560-10565.

[10] D. Ren, Y. L. Deng, A. D. Handoko, C. S. Chen, S. Malkhandi and B. S. Yeo, ACS Catal., 2015, 5, 2814-2821.

[11] J. J. Wu, S. C. Ma, J. Sun, J. I. Gold, C. S. Tiwary, B. Kim, L. Y. Zhu, N. Chopra, I. N. Odeh, R. Vajtai, A. Z. Yu, R. Luo, J. Lou, G. Q. Ding, P. J. A. Kenis and P. M. Ajayan, Nat. Commun., 2016, 7, 13869.

[12] Y. S. Zhou, F. L. Che, M. Liu, C. Q. Zou, Z. Q. Liang, P. De Luna, H. F. Yuan, J. Li, Z. Q. Wang, H. P. Xie, H. M. Li, P. N. Chen, E. Bladt, R. Quintero-Bermudez, T. K. Sham, S. Bals, J. Hofkens, D. Sinton, G. Chen and E. H. Sargent, Nat. Chem., 2018, 10, 974-980.

[13] T. T. Zhuang, Z. Q. Liang, A. Seifitokaldani, Y. Li, P. De Luna, T. Burdyny, F. L. Che, F. Meng, Y. M. Min, R. Quintero-Bermudez, D. Cao Thang, Y. J. Pang, M. Zhong, B. Zhang, J. Li, P. N. Chen, H. Y. Liang, W. N. Ge, B. J. Ye, D. Sinton, S. H. Yu and E. H. Sargent, Nat. Catal., 2018, 1, 421-428.

[14] Q. Zhang, J. Du, A. B. He, Z. H. Liu and C. Y. Tao, J. CO2 Util., 2019, 34, 635-645.

[15] J. Yuan, M. P. Yang, Q. L. Hu, S. M. Li, H. Wang and J. X. Lu, J. CO2 Util., 2018, 24, 334-340.

[16] J. Yuan, J. J. Zhang, M. P. Yang, W. J. Meng, H. Wang and J. X. Lu, Catal., 2018, 8, 171-181.